Metal Acetylacetonate Domains Grown on H-Terminated Porous Silicon at Room Temperature and Their Specific *I*−*V* Behavior

Jie Chao,[†] Hai-Tao Wang,[‡] Bing Xia,[†] Hong-Bo Liu,[†] Zhong-Dang Xiao,[‡] and Shou-Jun Xiao*,[†]

State Key Laboratory of Coordination Chemistry, School of Chemistry and Chemical Engineering, Nanjing University, Nanjing 210093, China, and State Key Laboratory of Molecular and Biomolecular Electronics, Southeast University, Nanjing 210096, China

Received: May 10, 2006; In Final Form: September 29, 2006

Porous silicon (PS) was incubated in an organic solution of metal acetylacetonates of $Mn(acac)_3$, $Fe(acac)_3$, $Co(acac)_3$, and $Ni(acac)_2$ (acac = MeCOCHCOMe) at room temperature. Crystal-like domains were found to be spontaneously self-assembled on PS surfaces by atomic force microscopy (AFM). Spectroscopic studies with attenuated total reflection Fourier transform infrared spectroscopy (ATR-FTIR) and X-ray photoelectron spectroscopy (XPS) revealed that the domains were grown from metal acetylacetonates. Current sensing atomic force microscopy (CSAFM) was used to measure the *I*−*V* curves of domains in nanoscale and specific step-jump currents on the manganese and cobalt acetylacetonate domains were surprisingly detected.

Introduction

Since Canham discovered the photoluminescence of nanocrystalline porous silicon (PS) in 1990,[1] PS has attracted much attention for its technological potential.[2,3] It is believed that PS will be used in light-emitting devices, catalysis, and chemical and biological sensing. Many organic species bearing functionalities of alkenes, alkynes, alkyl halides, acyl chlorides, Grignard reagents, and alkyllithium reagents had been used to assemble organic monolayers on silicon surfaces through the robust Si−C or Si−O−C bonds by heating, photoirradiation, microwave irradiation, electrochemical reduction, and Lewis acid catalysis.[4−8] It is obvious that a significant energy barrier for the conversion of surface Si−H to Si−C must be overcome with the assistance of extra energy. Are there any other chemical reagents that can be spontaneously self-assembled on H-terminated Si surfaces? During our work, we accidentally found that metal acetylacetonates can do so.

Metal acetylacetonates are a kind of coordination compounds bearing a positive metal ion in the center and 2 to 3 acetylacetone ligands coordinated to the metal ion.[9] In the earlier days, people studied their physical properties such as heat stability.[10,11] Nowadays, much attention has been paid to their characters of magnetism, electrics, and catalysis. For example, iron acetylacetonate was employed as a precursor to form magnetic nanoparticles,[12] manganese acetylacetonate was evaporated on silicon substrates as thin films for studies of their *I*−*V* character,[13] cobalt acetylacetonate was used as a catalyst for radical polymerization,[14] and nickel acetylacetonate was used for a selective reduction of an electronically deficient imine to amine in the presence of ketone with Et_2Zn together.[15]

During our investigation of surface tailoring of PS, we are looking for a gentle reaction to introduce functional species onto silicon. It is believed that a surface-propagated radical chain reaction contributes to the hydrosilylation.[16−19] We tried to introduce acetylacetonated compounds onto H-terminated PS. To our surprise, a series of metal acetylacetonates can be anchored spontaneously at room temperature. The formed membranes were characterized by ATR-FTIR, XPS, and atomic force microscopy (AFM) to confirm that the domains were grown from metal acetylacetonates. Finally, specific *I*−*V* curves of these domains grown on high-conducting silicon substrates were further measured by CSAFM. A step-jump current against sample bias was observed on Mn and Co acetylacetonate membranes. The so-called negative differential resistance (NDR) has been reported in a number of cases recently for molecular junctions. The d states of transition metals are higher in energy than π-bonding orbitals of the organic conjugated system, therefore the molecular electronic behavior could be realized much more easily on the self-assembled metal acetylacetonate membranes. Finally mechanisms for the spontaneous self-assembly and the specific electrical behavior were discussed.

Experimental Details

Sample Preparation. Single side polished silicon wafers (p-type, B-doped, (100) orientated, resistivity of 0.1−0.5 Ω cm, and 1.5 cm^2 exposed area) were boiled in 3:1 concentrated H_2SO_4/30% H_2O_2 for 30 min and then rinsed copiously with Milli-Q water (18 MΩ). A cleaned wafer was immersed in 1% aqueous HF solution for 1 min at room temperature to remove the native oxide. Then it was placed in a galvanic cell with the silicon as an anode and a Pt ring as the counter cathode (rotundity with the radius of about 6 mm to ensure a homogeneous electric field). Silicon was anodicly etched in ethanolic HF solution (3:1 (v/v) HF (40%)/ETOH) at a constant current density of 100 mA/cm^2 for 4 min. After etching, the wafer was rinsed with ethanol and dried with nitrogen. Metal acetylacetonate compounds [Mn(III)$(acac)_3$, Fe(III)$(acac)_3$, Co(III)$(acac)_3$, and Ni(II)$(acac)_2$] were synthesized and purified according to ref 11. $Mn(acac)_3$ or $Co(acac)_3$ (0.02 g) powder was dissolved in 10 mL of 1,3,5-methylbenzene, and the other two, $Fe(acac)_3$ and $Ni(acac)_2$, were dissolved in 1,4-dioxane (98%) with the same weight concentration. Freshly etched PS wafers were incubated in the metal acetylacetonate solution for 12 h, except

* Address correspondence to this author. Fax: 86-25-83314502. Phone: 86-25-83595706. E-mail: sjxiao@nju.edu.cn.
[†] Nanjing University.
[‡] Southeast University.

10.1021/jp0628481 CCC: $33.50
Published on Web 11/11/2006

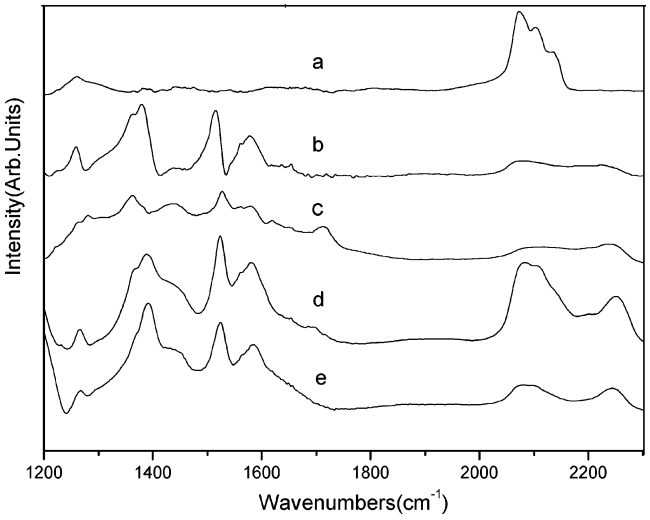

Figure 1. ATR-FTIR spectra of a freshly etched PS (a) and of PS modified with $Mn(acac)_3$ (b), $Fe(acac)_3$ (c), $Co(acac)_3$ (d), and $Ni(acac)_2$ (e). For clarity, the range of wavenumbers is plotted from 2300 to 1200 cm^{-1}.

TABLE 1: Frequencies and Assignments of IR Bands on Freshly Etched PS (a) and on PS Surfaces Modified with $Mn(acac)_3$ (b), $Fe(acac)_3$ (c), $Co(acac)_3$ (d), and $Ni(acac)_2$ (e)[a]

frequency (cm^{-1})					
a	b	c	d	e	assignment
	2246 (w)	2246 (w)	2250 (s)	2244 (m)	$(O_3)Si-H$ str
2137 (s)					sym $Si-H_3$ str
2103 (s)			2107 (w)	2104 (w)	sym $Si-H_2$ str
2072 (s)	2082 (w)	2083 (w)	2083 (s)	2082 (m)	sym Si−H str
	1577 (m)	1581 (w)	1581 (s)	1584 (s)	C═O str
	1515 (s)	1527 (m)	1524 (s)	1523 (s)	C═C str
	1442 (w)	1442 (w)	1444 (w)	1442 (w)	asym C−H bend
	1378 (s)	1363 (m)	1389 (s)	1392 (s)	sym C−H bend
	1259 (m)	1259 (w)	1266 (m)	1267 (m)	C═C−H in-plane bend

[a] Abbreviations: sym, symmetric; asym, asymmetric; s, strong; m, medium; w, weak; str, streching; bend, bending.

for 4 h in the $Mn(acac)_3$ solution. After incubation, the wafers were sonicated in the same solvent of its corresponding reaction solution for 10 min, rinsed with ethanol, and dried with nitrogen.

ATR-FTIR Spectroscopy. Attenuated total reflection Fourier transform infrared spectra were recorded with a Pike accessory MIRacle ATR in a Bruker IFS66/S spectrometer at 1 cm^{-1} resolution. Typically 128 interferograms were acquired per spectrum. The surface of samples was put onto a ZnSe crystal in a sample chamber purged with dry air. Air was used to obtain the background spectrum. Peaks of carbon dioxide and water were eliminated with the software.

XPS Spectroscopy. XPS (VG, ESCALB MK-II), which has a monochromatized Mg Kα X-ray source (300 W), was employed to analyze the surfaces. The round porous silicon sample with a diameter of 1.0 cm was embedded in a Ni substrate with double glue. Survey scans (Constant Analyzer Energy (CAE) = 100 eV, step = 0.50 eV) over a binding energy of 0−1150 eV were run for the elemental information, and followed with high-resolution scans of C 1s, O 1s, Me(metal) 2p, and Si 2p (CAE = 20 eV, step = 0.05 eV) to determine binding energies and atomic concentrations. All binding energies were normalized to Si(metal) 2p at 99.0 eV. Measurements were carried out with a take-off angle of 45° with respect to the sample surface. Peak-fitting was done with ESCALB MK-II software.

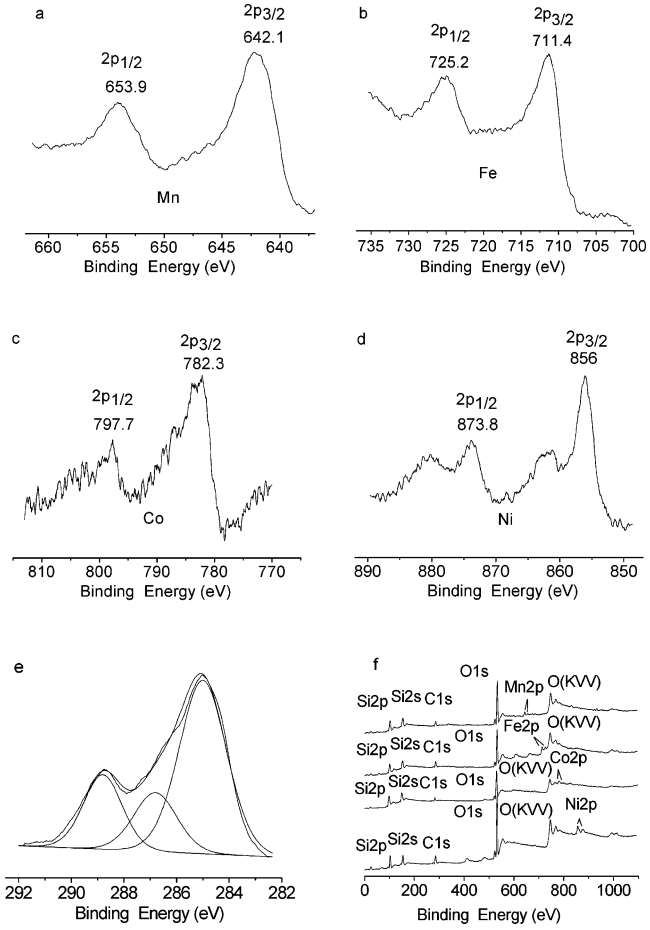

Figure 2. High-resolution XPS spectra of (a) Mn2p from Mn-$(acac)_3$modified-, (b) Fe2p from $Fe(acac)_3$-modified, (c) Co2p from Co-$(acac)_3$-, and (d) Ni2p from $Ni(acac)_2$-modified PS samples, of C1s from $Fe(acac)_3$-modified PS (e), and survey spectra of four metal acetylacetonated PS samples (f).

Atomic Force Microscopy. A Nanoscope IIIA AFM (Digital Instruments) was used to analyze the topography of the sample immediately after etching or reaction to minimize the contamination on the surface. The AFM was operated in contact mode and the Digital Nanoscope software version 5.12b was used to analyze the surface roughness profiles of the samples.

Current Sensing AFM. All current sensing AFM operations were carried out on a Multimode SPM with the PicroSPM II controller (Molecular Imaging, Temp, AZ). AFM imaging was done under ambient conditions (with a relative humidity of 20% at 26 °C), using a contact mode AFM with 20 nm Au-coated commercial Si cantilevers (MikroMasch USA). Generally, samples were swept from positive to negative.

Results and Discussion

The IR spectra of a control sample PS (a) and of $Mn(acac)_3$-(b), $Fe(acac)_3$- (c), $Co(acac)_3$- (d), and $Ni(acac)_2$-modified PS (e) are shown in Figure 1. The frequencies and their assignments are listed in Table 1. The spectrum of the freshly etched PS exhibited a typical tripartite band for $Si-H_x$ ($x = 1-3$) stretching modes (2072 cm^{-1} for νSi−H, 2103 cm^{-1} for $\nu Si-H_2$, and 2137 cm^{-1} for $\nu Si-H_3$). After reaction, the obvious change is the appearance of new peaks between 1200 and 1700 cm^{-1}. Due to the same ligand, metal acetylacetonates have almost the same IR peaks which are 1581 cm^{-1} for νC═O, 1524 cm^{-1} for νC═C, 1442 cm^{-1} for δ_{as}C−H, 1380 cm^{-1} for δ_sC−H, and 1260 cm^{-1} for δC═C−H. Another change in IR spectra

TABLE 2: The Ratios of Carbon/Metal, Oxygen/Metal, and Silicon/Metal Corresponding to (a) $Mn(acac)_3$-, (b) $Fe(acac)_3$-, (c) $Co(acac)_3$-, and (d) $Ni(acac)_2$-Modified PS Samples

	a	b	c	d
C/metal	3.73	3.95	4.92	5.14
O/metal	10.15	8.72	16.38	12.50
Si/metal	6.12	5.59	16.46	6.17

is the evolution of $Si-H_x$, where a new $(O_3)Si-H$ stretching band appears at 2246 cm^{-1} and two old bands at 2082 cm^{-1} from Si−H and 2103 cm^{-1} from $Si-H_2$ are still observable but with lower intensity in spectra b−e of Figure 1.

High-resolution XPS spectra in Figure 2 show metal elements of (a) Mn2p (2p3/2 at 642.1 eV and 2p1/2 at 653.9 eV), (b) Fe2p (2p3/2 at 711.4 eV and 2p1/2 at 725.2 eV), (c) Co2p (2p3/2 at 782.1 eV and 2p1/2 at 797.7 eV), and (d) Ni2p (2p3/2 at 856.0 eV and 2p1/2 at 873.8 eV), on their corresponding metal acetylacetonate PS surfaces, respectively. Since all modified surfaces have the same ligand, acetylacetonate, only one high-resolution C1s on $Fe(acac)_3$-modified PS is shown in Figure 2e. The C 1s envelope is deconvoluted into three peaks: a main peak centered at 285.0 eV (60.21%) due to hydrocarbon containing both alkyl carbon in acetylacetonate and a trace of hydrocarbon contaminants, a peak at 286.6 eV (18.61%) due to enol ═C−OH carbon, and another one at 288.8 eV (21.18%) due to the carbonyl (C═O) carbon.[20] However, the C1s of the $Fe(acac)_3$ powder sample (Figure S2 in the Supporting Information) shows 3 peaks at 285.0 (63.40%), 286.6 (17.61%), and 287.3 eV (18.99%). Both enol and carbonyl groups coordinated to iron are via the oxygen atom. The 1.5 eV shift of the third peak of the surface C1s from its corresponding powder should be caused by the change of molecular structure from powder-$Fe(acac)_3$ to surface-$(Fe(acac)O)_n$, where an asymmetric single acac ligand coordinates to iron on the surface (Scheme 3). The survey spectra of metal acetylacetonate PS surfaces are shown in Figure 2f and their atomic ratios C/metal, O/metal, and Si/metal on each surface are listed in Table 2, respectively. Three issues are addressed: (1) Silicon is always present on the surface and it exists as both Si−Si (38.41% for a, 84.11% for b, 56.77% for c, and 17.10% for d) and Si−O (61.59% for a, 15.89% for b, 43.23% for c, and 82.90% for d) states (see Figure S3 and Table S1 in the Supporting Information). Since the AFM imaging (Figure 3) tells us that crystal-like domains are higher than 10 nm and spread on the surface separately, we suggest that the signal of silicon come from the valley area, where Si−H species are oxidized to SiO_2 with a thickness less than 6 nm. The metal acetylacetonate species aggregate favorably on reactive sites rather than deposit homogeneously on the whole surface. (2) The carbon/metal ratio, close to 5, indicates that each metal atom finally binds one acac ligand and two other acac ligands leave during the surface deposition. (3) The ratio of oxygen/metal is much higher than the ideal 1 acac/metal ratio of 2. An integrated analysis of IR, XPS, and AFM results suggests that oxygen atoms from solution replace 2 acac ligands during the domain growth. Therefore the surface oxygen exists in three forms: oxygen in acac coordinated to metal ions, an oxygen bridge between metal atoms, and silicon oxide. These kinds of surface reactions with unstable acac ligands taken from the metal by oxygen can be supported by other literature.[21]

Except for the IR and XPS spectroscopy measurements, the topographies of modified surfaces were imaged by AFM in Figure 3. The top-view AFM images of freshly etched PS (a) and PS surfaces modified with (b) $Mn(acac)_3$, (c) $Fe(acac)_3$, (d) $Co(acac)_3$, and (e) $Ni(acac)_2$ were analyzed with linear cross-section profiles, respectively. The control sample PS with a 2 × 2 μm^2 image exhibits a relatively flat area, where the distance between two red arrows was 195.0 nm, which contains 9 pores

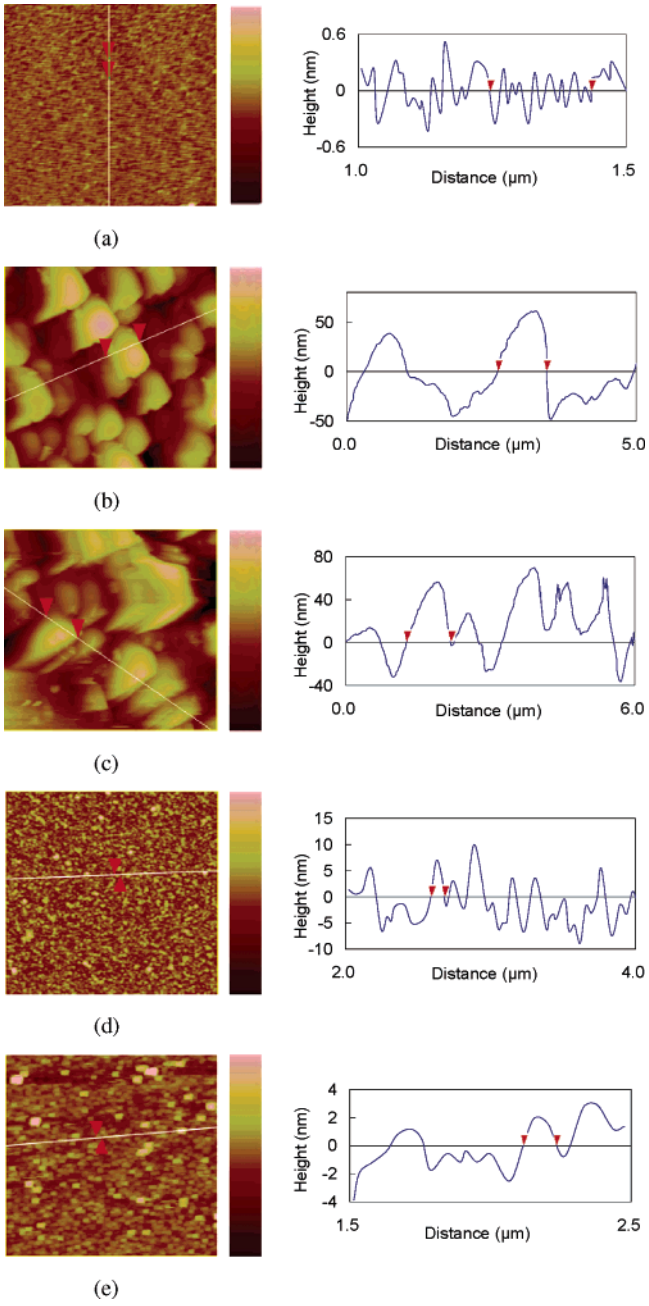

Figure 3. Top-view AFM images and their corresponding linear cross-section profiles taken along the marked segments of freshly etched PS (a) (2 × 2 μm^2) and surfaces modified with (b) $Mn(acac)_3$ (5 × 5 μm^2), (c) $Fe(acac)_3$ (5 × 5 μm^2), (d) $Co(acac)_3$ (5 × 5 μm^2), and (e) $Ni(acac)_2$ (5 × 5 μm^2). For clarity, only a part of the linear cross-section profiles (height against selected distance in a marked segment) were listed here.

SCHEME 1: Schematic Setup of *I*−*V* Measurements on a PS-Based Metal Acetylacetonate Domain[a]

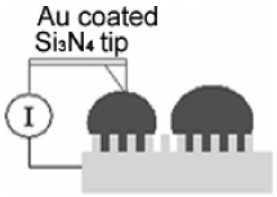

[a] An Au-coated CSAFM tip was placed on the top of the domain.

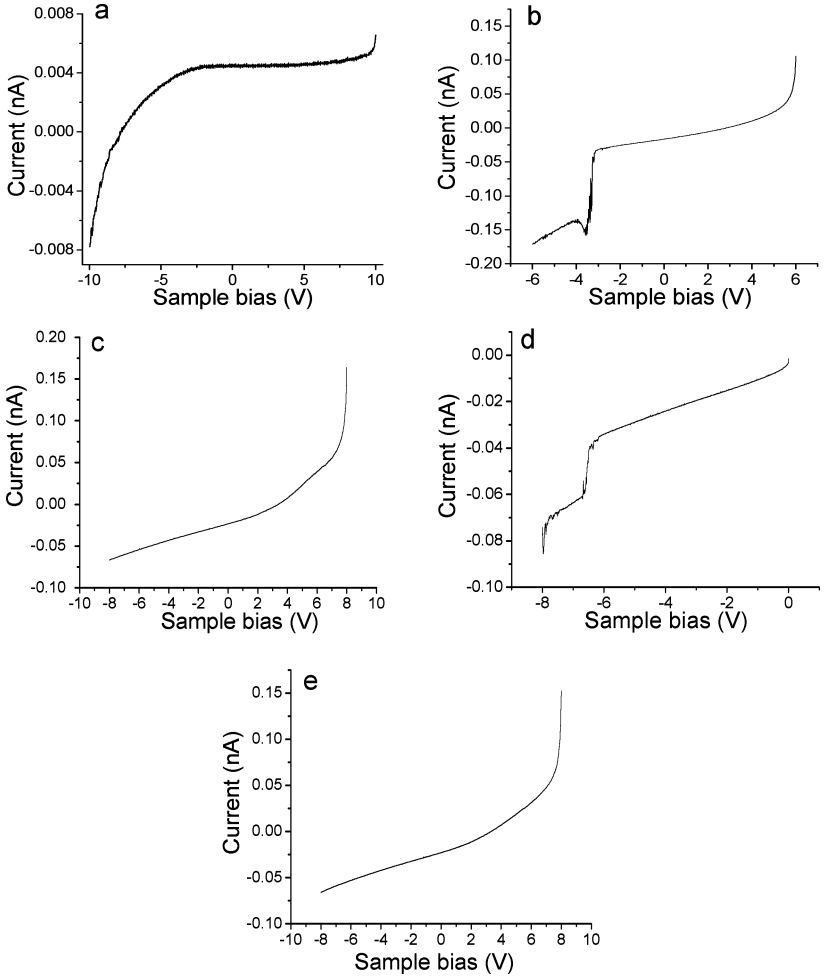

Figure 4. Typical $I-V$ curves measured on freshly prepared PS (a), and surfaces modified with (b) $Mn(acac)_3$, (c) $Fe(acac)_3$, (d) $Co(acac)_3$, and (e) $Ni(acac)_2$. Curve a exhibits the rectification at the negative sample bias, curves b and d present steplike jump features, and curves c and e show the rectification at the positive sample bias. For clarity, the ranges of sample bias were set differently.

and 8 clearances. Suppose that pores and clearances have the same size and the average diameter of the pores is 11.5 nm. The domains of Mn and Fe acetylacetonate surfaces in Figure 3b−e have sharp edges and look like small crystals. Their domain sizes can be estimated with the linear cross-section profiles as roughly 921.3 (width) × 60.0 (height) nm^2 in panel b and 913.1 (width) × 50.0 (height) nm^2 in panel c by measuring the cross-section profiles between two red arrows, respectively. Unlike Mn and Fe acetylacetonate surfaces, the domains of Co and Ni acetylacetonate surfaces in Figure 3d−e are much smaller. The Ni acetylacetonate domains (e) exhibit a cubic shape but Co acetylacetonate domains (d) only present random shapes. The average size of domains is 98.8 (width) × 5.0 (height) nm^2 in panel d and 136.8 (width) × 3.0 (height) nm^2 in panel e, respectively. From these AFM images, we can conclude that domains but not monolayers are deposited on PS surfaces. In other words, metal acetylacetonates self-assembled on PS by chemical binding first followed by radical polymerization.

The schematic setup for $I-V$ measurements is shown in Scheme 1. XPS spectra and AFM images point to the inhomogeneous deposition of metal acetylacetonate domains on surfaces. The dark bumps correspond to domains while the valley area is covered by an ultrathin SiO_2 layer from oxidation of Si−H species. A schematic structure of metal−acetylacetonated domains on PS is shown in Scheme 3. Typical $I-V$ curves of metal acetylacetonate domains on PS were measured with CSAFM in Figure 4. PS itself exhibits an n-type rectification

SCHEME 2: Common Structure of Metal Acetylacetonate

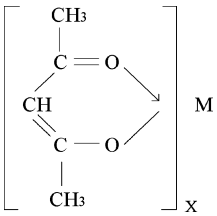

at the negative sample bias. However, we used p-Si as the substrate. The seeming controversy can be interpreted possibly as that the porous silicon membrane was etched to form a PS/p-Si junction. Two samples, Mn and Co acetylacetonate domains, exhibit the steplike jump of currents in panels b and d of Figure 4, respectively. Mn acetylacetonate domains (Figure 4b) present the steplike change from −3.03 V to −3.98 V when the sample bias was sweeping down from 0.00 V to −6.00 V, while in the case of Co acetylacetonate domains (Figure 4d), the sudden change occurs from −6.40 V to −6.70 V when the sample bias was sweeping down from 0.00 V to −8.00 V. The current jumps in the above two cases correspond to a sudden increase of conductance through the heterogeneous junctions. The probability of the steplike jump phenomena is 86.5% for Mn- and 70.3% for Co acetylacetonate domains. Six hundred measurements were done on 15 different samples for each case. By repeating the sweep at the same site, the $I-V$ curves are still reproducible except that the jump may occur at a locally

SCHEME 3: The Possible Reaction Mechanism of H-Terminated Porous Silicon with Metal Acetylacetonate[a]

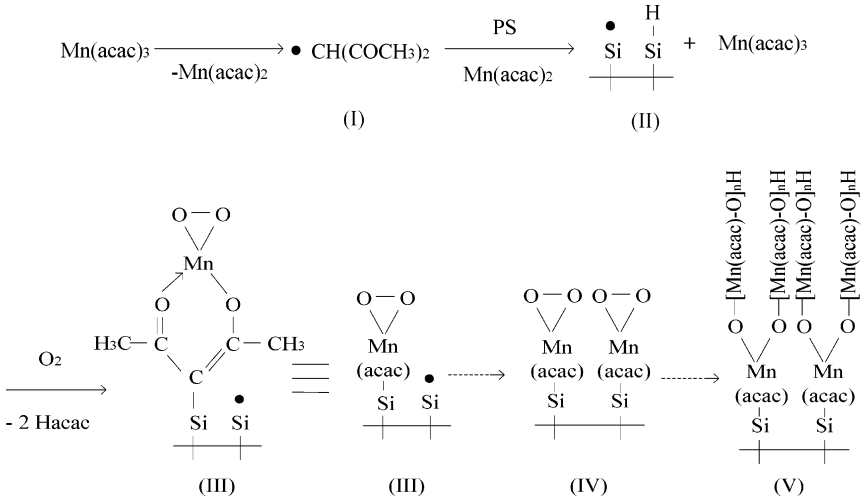

[a] Take manganese acetylacetonate, for example, and see text for interpretation.

shifted bias. The step height for Mn acetylacetonate is 0.15 ± 0.01 nA and that for Co acetylacetonate is 0.020 ± 0.005 nA, respectively. Reports of nonlinear current−voltage relationships due to molecular geometric changes[22] or due to bond breaking[23] have also been reported. Among research on molecular junctions in a metal−molecule−metal system, the scanning probe was generally used as one metal electrode while the other metal electrode was usually Au, highly oriented pyrolitic graphite (HOPG), or silicon with good conductance.[24] A mechanism, consistent with the theory proposed by Datta,[25] involved the tuned alignment of molecular energy levels with a narrow band of conducting electrons or holes in degenerately doped n- or p-type silicon, respectively. A theoretical calculation demonstrated that the current change (also called negative differential resistance (NDR) effect) was positive in the probe−molecule−silicon (p-type) system and negative when silicon was n-type doped.[26] Pitters et al. pointed out the complication of $I-V$ phenomena and proposed that a structure change might be involved.[27] Qiu et al. studied the current-jump phenomenon in the $I-V$ curve of a Zn(II) etioporphyrin I monolayer on NiAl (110) surface by STM and ascribed it to the intraconversion between two conformations of Zn(II) etioporphyrin.[28] Olivier et al. investigated the $I-V$ characters of freshly cleaved transition-metal dichalcogenides whose resistivities are sensitive to temperature changes with CSAFM and proposed that the distortions of $I-V$ curves such as step-jumps were due to Joule heating.[29] We would prefer the latter interpretation of Joule effect for our observed step-jump phenomena in Figure 4a,c because of the higher sample bias up to ∼6.0 V. Panels c and e of Figure 4 illustrate the $I-V$ characters of Fe and Ni acetylacetonate domains on PS, respectively. Contrary to curves of Figure 4b,d, they only show the p-type rectification at the positive bias, different from the n-type rectification on H-terminated PS. We suggest that the doping of Fe and Ni acetylacetonate into PS may alter the PS structure and therefore the whole system presents the p-type behavior again. Actually until now, the different $I-V$ characters on individual surfaces have not yet been fully understood. Further investigation is still in progress.

According to ref 11, the common structure of metal acetylacetonate and the method of metal coordination is shown in Scheme 2. Metal acetylacetonates are usually used as radical initiators[30] in organic reactions. We propose a mechanism for the spontaneous assembly in Scheme 3. The decomposition of $Mn(acac)_3$ would produce a diacetylmethyl radical (I) and it attacks the Si−H bond, resulting in a silicon radical (**II**) and $Mn(acac)_3$. Then, the silicon radical (**II**) attacks the carbon of the double bond in $Mn(acac)_3$ to anchor the metal acetylacetonate and the radical propagates to the next silicon atom; O_2 from the environment also participates in the reaction to replace the other two acetylacetonate ligands (**III**). With the propagation of the silicon radical on the surface, a localized intermediate $Mn(acac)O_2$ peroxide layer is formed (**IV**). The peroxide is unstable and it is easily initiated by acac radicals to polymerize and a polymer structure with a Mn(acac)-O unit is proposed as **V**. The terminal peroxide bond is hydrolyzed to a hydroxyl group. The domain structure is due to the localized polymerization.

In conclusion, freshly etched porous silicon can react with acetylacetonates of manganese, iron, cobalt, and nickel spontaneously at room temperature. Domains with different sizes were observed with AFM. Spectroscopic studies of IR and XPS confirmed that they were grown from metal acetylacetonates. The $I-V$ measurements of domains on nanoscale by CSAFM revealed the rectification behavior on naked PS samples toward the negative sample bias, and on Fe and Ni acetylacetonate domains toward the positive bias. More surprisingly, steplike jump currents on Mn and Co acetylacetonate domains were detected toward the negative sample bias. With introducing metal elements into PS, its characters of electrics, optics, and magnetics will be improved and therefore potential applications will be widened.

Acknowledgment. The authors thank Mr. Hong-Qi Shi and Ms. Xiao-Shu Wang for their help in FITR and XPS measurements, respectively. This work was supported by NSFC No. 20571042.

Supporting Information Available: IR and XPS C1s spectra of $Fe(acac)_3$ powder, Si2p spectra of each metal acetylacetonated PS surface and the corresponding deconvolution of Si(−Si) and Si(−O). This material is available free of charge via the Internet at http://pubs.acs.org.

References and Notes

(1) Canham, L. T. *Appl. Phys. Lett.* **1990**, *57*, 1046−1048.

(2) Canham, L. T. *Properties of Porous Silicon*; Academic: London, UK, 1997.

(3) Stewart, M. P.; Buriak, J. M. *Adv. Mater.* **2000**, *12*, 859−869.

(4) (a) Linford, M. R.; Fenter, P.; Eisenberger, P. M.; Chidsey, C. E. D. *J. Am. Chem. Soc.* **1995**, *117*, 3145−3155. (b) Buriak, J. M. *Chem. Commun.* **1999**, 1051−1060.

(5) (a) Boukherroub, R.; Morin, S.; Bensebaa, F.; Wayner, D. D. M. *Langmuir* **1999**, *15*, 3831−3835. (b) Boukherroub, R.; Wayner, D. D. M. *J. Am. Chem. Soc.* **1999**, *121*, 11513−11515.

(6) (a) Sieval, A. B.; Vleeming, V.; Zuilhof, H.; Sudholter, E. J. R. *Langmuir* **1999**, *15*, 8288−8291. (b) Haber, J. A.; Lauermann, I.; Michalak, D.; Vaid, T. P.; Lewis, N. S. *J. Phys. Chem. B* **2000**, *104*, 9947−9950.

(7) (a) Cicero, R. L.; Linford, M. R.; Chidsey, C. E. D. *Langmuir* **2000**, *16*, 5688−5695. (b) Boukherroub, R.; Morin, S.; Sharpe, P.; Wayner, D. D. M.; Allongue, P. *Langmuir* **2000**, *16*, 7429−7434.

(8) (a) Niederhauser, T. L.; Lua, Y. Y.; Sun, Y.; Jiang, G.; Strossman, G. S.; Pianetta, P.; Linford, M. R. *Chem. Mater.* **2002**, *14*, 27−29. (b) Lie, L. H.; Patole, S. N.; Hart, E. R.; Houlton, A.; Horrocks, B. R. *J. Phys. Chem. B* **2002**, *106*, 113−120. (c) Lees, I. N.; Lin, H.; Canaria, C. A.; Gurtner, C.; Sailor, M. J.; Miskelly, G. M. *Langmuir* **2003**, *19*, 9812−9817.

(9) Urbain, G.; Debierne, A. *C. R. Hebd. Seances Acad. Sci.* **1899**, *129*, 302−303.

(10) Bailar, J. C., Jr. *The Chemistry of the Coordination Compounds*; Academic: New York, 1956.

(11) Robert, G.; Charles, M. *J. Phys. Chem.* **1958**, *62* (3), 440−444.

(12) Zhang, L.; He, R.; Gu, H. C. *Mater. Res. Bull.* **2006**, *41*, 260−267.

(13) Dakhel, A. A. *J. Non-Cryst. Solids* **2005**, *351*, 3204−3208.

(14) Christophe, D.; Antoine, D.; Rayna, B.; Bernadette, C.; Robert, J.; *Macromol. Rapid Commun.* **2006**, *27*, 37−41.

(15) Xiao, X.; Wang, H. W.; Huang, Z. Y. *Org. Lett.* **2006**, *8*, 139−142.

(16) Robins, E. G.; Stewart, M. P.; Buriak, J. M. *Chem. Commun.* **1999**, 2479−2480.

(17) Gurtner, C.; Wun, A. W.; Sailor, M. J. *Angew. Chem., Int. Ed. Engl.* **1999**, *38*, 1966−1968.

(18) Schmeltzer, J. M.; Porter, J. L. A.; Stewart, M. P.; Buriak, J. M *Langmuir* **2002**, *18*, 2971−2974.

(19) Linford, M. R.; Chidsey, C. E. D. *J. Am. Chem. Soc.* **1993**, *115*, 12631−12632.

(20) Kodolov, V. J.; Tchirkova, E. I.; Bystrova, S. G.; Shabanova, I. N.; Popova, O. V.; Babushkina, S. N. *J. Electron Spec. Relat. Phenom.* **1998**, *88*, 997−982.

(21) Van Der Voort, P.; Van Welzenis, R.; De Ridder, M.; Brongersma, H. H.; Baltes, M.; Mathieu, M.; van de Ven, P. C.; Vansant, E. F. *Langmuir* **2002**, *18*, 4420−4425.

(22) (a) Donhauser, Z. J.; Mantooth, B. A.; Kelly, K. F.; Bumm, L. A.; Monnell, J. D.; Stapleton, J. J.; Price, D. W., Jr.; Rawlett, A. M.; Allara, D. L.; Tour, J. M.; Weiss, P. S. *Science* **2001**, *292*, 2303−2307. (b) Gaudioso, J.; Lauhon, L. J.; Ho, W. *Phys. Rev. Lett.* **2000**, *85*, 1918−1921. (c) Gaudioso, J.; Ho, W. *Angew. Chem., Int. Ed.* **2001**, *40*, 4080−4082. (d) Hla, S. W.; Meryer, G.; Rieder, K. H. *Chem. Phys. Lett.* **2003**, *370*, 431−436. (e) Yang, G.; Liu, G. Y. *J. Phys. Chem. B* **2003**, *107*, 8746−8759.

(23) (a) Selzer, Y.; Salomon, A.; Ghabboun, J.; Cahen, D. *Angew. Chem., Int. Ed.* **2002**, *41*, 827−830. (b) Salomon, A.; Arad-Yellin, R.; Shanzer, A.; Karton, A.; Cahen, D. *J. Am. Chem. Soc.* **2004**, *126*, 11648−11657.

(24) (a) Guisinger, N. P.; Greene, M. E.; Basu, R.; Baluch, A. S.; Hersam, M. C. *Nano Lett.* **2004**, *4*, 55−59. (b) Guisinger, N. P.; Basu, R.; Greene, M. E.; Baluch, A. S.; Hersam, M. C. *Nanotechnology* **2004**, *15*, S452−S.458.

(25) Rakshit, T.; Liang, G. C.; Ghosh, A. W.; Datta, S. *Nano Lett.* **2004**, *4*, 1803−1807.

(26) Rakshit, T.; Liang, G. C.; Ghosh, A. W.; Datta, S. *J. Comput. Electron.* **2005**, *4*, 83−86.

(27) Pitters, J. L.; Wolkow, R. A. *Nano Lett.* **2006**, *6*, 390−397.

(28) Qiu, X. H.; Nazin, G. V.; Ho, W. *Phys. Rev. Lett.* **2004**, *93*, 196806.

(29) Olivier, S.; Alec, M.; Kang, W.; Annie, L.; Philippe, M. *J. Phys. Chem. B* **2006**, *110*. 9991−9994.

(30) Nishini, H.; Tategami, S.; Yamada, T.; Korp, J. D.; Kurosawa, K. *Bull. Chem. Soc. Jpn.* **1991**, *64*, 1800−1809.